# A Third-Generation Model for Wind Waves on Slowly Varying, Unsteady, and Inhomogeneous Depths and Currents

HENDRIK L. TOLMAN

*Department of Civil Engineering, Delft University of Technology, Delft, The Netherlands*

(Manuscript received 6 July 1990, in final form 28 November 1990)

ABSTRACT

A full discrete spectral model for propagation, generation and dissipation of wind waves for arbitrary depth, current and wind fields is presented (WAVEWATCH). This model incorporates all relevant wave–current interaction mechanisms, including changes of absolute frequencies due to unsteadiness of depth and currents. The model furthermore explicitly accounts for growth and decay of wave energy and for nonlinear resonant wave–wave interactions. The numerical schemes for propagation are basically second-order accurate. Effects of refraction and frequency shifts (due to unsteadiness of depth and current) are calculated on a fixed grid, also using second-order schemes. This paper focuses on the governing equations and the numerical algorithms. Furthermore some results for academic and realistic cases are presented to illustrate some features and merits of the model.

## 1. Introduction

In the last few decades operational models have been developed for predicting or hindcasting wind waves and currents, ignoring interactions between them. However, effects of currents on waves have long been recognized by people living near the coast and by sailors (e.g., the existence of tidal races, i.e., current-induced severe wave breaking, near inlets and headlands and on shoals). This close relationship has also been recognized theoretically. After some pioneering papers by Unna (1941, 1942, 1947) and Barber (1949), the theory for wave–current interaction was developed by Longuet-Higgins and Stewart (1960, 1961, 1962), who introduced the concept of radiation stress, and by Whitham (1965) and Bretherthon and Garrett (1968), who introduced the concept of action conservation. The theory is well established and it is treated in various textbooks, review papers and reports (e.g., Whitham 1974; Peregrine 1976; Phillips 1977; Mei 1983; Peregrine and Jonsson 1983; Jonsson 1990).

Several numerical wave models have been developed for waves on currents (e.g., Tayfun et al. 1976; Radder 1979; Sakai et al. 1983; Chen and Wang 1983; Mathiesen 1987; Holthuijsen et al. 1989), usually for relatively small scale (coastal) areas. Some models (or combinations of models) also incorporate the effects of wind waves on currents (Skovgaard and Jonsson 1976; extended by Christoffersen 1982; Dingemans et al. 1986). However, these models have been developed for (quasi-) stationary depths and currents for which changes of absolute frequency due to the unsteadiness of depth and current can be neglected.[1] Furthermore source terms for wave generation, dissipation and nonlinear wave–wave interactions are highly parameterized, if considered at all in such models.

The description of wave generation, dissipation and nonlinear wave–wave interactions is much more developed in ocean wave models. After the pioneering work of Gelci et al. (1956, 1957), several such models have been developed (see e.g., SWAMP Group 1985; SWIM Group 1985). These models are denoted as first, second or third generation wave models, depending on the level of parameterization of generation, dissipation and nonlinear wave–wave interactions (see e.g., WAMDI Group 1988). The highest level of development is presently reached in the third-generation WAM model (WAMDI Group 1988), in which all processes of wave generation, dissipation and nonlinear wave–wave interactions are accounted for explicitly. Wave–current interactions, however, are not incorporated in this or any other ocean wave model.

In several situations waves propagate over current fields with length scales on which generation is important (i.e., of the order of 100–1000 km), for instance, tides in shelf seas or deep-ocean currents like the Gulf Stream. Furthermore currents on these large scales can be unsteady. To account for wave–current interactions

*Corresponding author address:* Dr. H. L. Tolman, Code 911, NASA/Goddard Space Flight Center, Greenbelt, MD 20771.

[1] Parallel to the development of WAVEWATCH, Yamaguchi et al. (1989) and Yamaguchi and Hatada (1990) developed ray models for propagation of irregular waves on unsteady and inhomogeneous currents (neglecting source terms).

in such unsteady conditions, the unsteadiness has to be fully accounted for (e.g., Tolman 1990b). To the knowledge of the present author, no model for wind waves on such large scale (potentially unsteady) currents was available. Such a model (WAVEWATCH) is presented here.

The present model combines the advanced propagation formulations of coastal wave models (depth and current refraction, energy exchange with the mean current), with the source term formulations of ocean wave models. The numerical techniques (i.e., solution of an action balance equation on a fixed grid) are mostly taken from ocean wave models, since the conventional wave ray technique of most coastal models is inconvenient to compute wave heights and (nonlinear) source terms.

The model has been developed to investigate effects of tides and surges on wind waves in shelf seas (thesis of the present author 1990a). The selection of numerical schemes and results of academic test cases are discussed in detail by Tolman (1989, 1990a). This paper focuses on the governing equations and the (final) numerical algorithms. Growth characteristics of WAVEWATCH will not be discussed here, since the formulation and treatment of the source terms is essentially identical to those of the WAM model (WAMDI Group 1988). To illustrate specific features of the present model, results for three example calculations are presented. First, results of a refraction test on a plane beach are presented to illustrate the performance of refraction by the second-order scheme and to discuss relevant aspects of previously published refraction schemes. Second, results of wave propagation over a Gulf Stream ring are presented to illustrate the advantages of a grid model (as used here) over a ray model for waves on currents. This case is treated in full by Holthuijsen and Tolman (1991). Third, some results of a hindcast for the North Sea are presented to illustrate the importance of the effects of unsteadiness of depth and current and to compare model behavior with observations. This case is taken from the study, for which WAVEWATCH has been developed (Tolman 1990a, 1991a).

## 2. Governing equations

### a. Introduction

The governing equations for wind wave propagation and generation are well established, as discussed in the introduction. Formulations as used in the model described here are summarized below for completeness only. A detailed description of the theory can be found in the textbooks and review papers mentioned in the introduction.

Wind waves are usually described with a variance density $F$ as a function of wave phase parameters such as the wavenumber $k$, the intrinsic or relative frequency $\sigma$ (as observed in a frame of reference moving with the mean current $\mathbf{U}$), the absolute frequency $\omega$ (as observed in a fixed frame) and the direction $\theta$ (normal to the wave crest of the component). In the linear theory for (quasi-) uniform surface gravity waves on slowly varying depths and currents (e.g., Whitham 1974; Phillips 1977; LeBlond and Mysak 1978), the wavenumber $k$ is related to the frequencies $\sigma$ and $\omega$ in the dispersion relation (surface tension neglected):

$$\sigma = \sqrt{gk \tanh kd} = \omega - \mathbf{k} \cdot \mathbf{U}, \tag{1}$$

where $g$ is the acceleration of gravity, $d$ is the water depth (average over the wave field) and $\mathbf{k}$ is the wavenumber vector with magnitude $k$ and direction $\theta$. With this $\omega - k$ relation, the spectrum is essentially two-dimensional. This spectrum is denoted here as $F(\ell)$, where $\ell$ denotes the two independent spectral variables (chosen from $\mathbf{k}$, $k$, $\theta$, $\omega$ and $\sigma$). For the moment no specific choice of independent spectral parameters will be made. At the scale of wave propagation, the spectrum is also a function of location $\mathbf{x}$ and time $t$, so that the spectrum is essentially five-dimensional, i.e. $F(\ell, \mathbf{x}, t)$.

If waves propagate over slowly varying depths and currents, the linear uniform-wave theory remains (locally) applicable. Changes of the wavenumber $k$, frequencies $\sigma$ and $\omega$ and direction $\theta$ during propagation can be determined from the kinematics of wave trains. Changes of the spectral density during propagation can be determined using energy or action conservation equations. Diffraction will be ignored altogether.

### b. Kinematics

In the linear wave theory the variance (energy) of wave components travels with the group velocity given by

$$\frac{d\mathbf{x}}{dt} = \mathbf{c}_g + \mathbf{U}, \tag{2}$$

$$c_g = n\frac{\sigma}{k}, \quad n = \frac{1}{2} + \frac{kd}{\sinh^2 kd}. \tag{3}$$

The rates of change of absolute frequency $\omega$, wavenumber $k$, relative frequency $\sigma$ and direction $\theta$ while moving with this velocity $\mathbf{c}_g + \mathbf{U}$, denoted as $d\omega/dt$, $dk/dt$, $d\sigma/dt$ and $d\theta/dt$, respectively, are (e.g., Christoffersen 1982; Mei 1983, p. 96):

$$\frac{d\omega}{dt} = c_\omega = \frac{\partial\sigma}{\partial d}\frac{\partial d}{\partial t} + \mathbf{k} \cdot \frac{\partial \mathbf{U}}{\partial t}, \tag{4}$$

$$\frac{dk}{dt} = c_k = -\frac{\partial\sigma}{\partial d}\frac{\partial d}{\partial s} - \mathbf{k} \cdot \frac{\partial \mathbf{U}}{\partial s}, \tag{5}$$

$$\frac{d\sigma}{dt} = c_\sigma = \frac{\partial\sigma}{\partial d}\left[\frac{\partial d}{\partial t} + \mathbf{U}\cdot\nabla_x d\right] - c_g\mathbf{k}\cdot\frac{\partial \mathbf{U}}{\partial s}, \quad (6)$$

$$\frac{d\theta}{dt} = c_\theta = -\frac{1}{k}\left[\frac{\partial\sigma}{\partial d}\frac{\partial d}{\partial m} + \mathbf{k}\cdot\frac{\partial \mathbf{U}}{\partial m}\right], \quad (7)$$

in which $s$ is the space coordinate in the direction $\theta$ and $m$ is a coordinate normal to $s$; $\nabla_x$ is the two-dimensional differential operator in the x-space and the operator $d/dt$ is defined as

$$\frac{d}{dt} = \frac{\partial}{\partial t} + [\mathbf{c}_g + \mathbf{U}]\cdot\nabla_x. \quad (8)$$

The quantities $c$ in the above equations will be used in the following as propagation speeds in the spectral space. Note that since Eq. (1) provides a local relation between the wavenumber and the frequencies, only one of the Eqs. (4) through (6) has to be integrated to obtain $\omega$, $\sigma$ and $k$.

### c. Dynamics

In cases without currents the change of wave height during propagation is determined using an energy conservation equation (Whitham 1974; Phillips 1977; Mei 1983). In cases with currents, the wave energy is generally not conserved, since the mean horizontal momentum transport of the waves (i.e., the radiation stress) causes an exchange of energy with the mean current (Longuet-Higgins and Stewart 1961, 1962). In such conditions, the wave action $N = F/\sigma$ is conserved during propagation (e.g., Whitham 1965; Bretherthon and Garrett 1968). This is the basis for the spectral action balance equation (e.g., Hasselmann et al. 1973; Willebrand 1975):

$$\frac{\partial N(\ell, \mathbf{x}, t)}{\partial t} + \nabla_x\cdot\left[\frac{d\mathbf{x}}{dt}N(\ell, \mathbf{x}, t)\right] + \nabla_\ell\cdot\left[\frac{d\ell}{dt}N(\ell, \mathbf{x}, t)\right] = \frac{S(\ell; \mathbf{x}, t)}{\sigma}, \quad (9)$$

where $N(\ell, \mathbf{x}, t)$ is the action density spectrum, $\nabla_\ell$ is the two-dimensional differential operator in the $\ell$-space and $d\ell/dt$ is the two-dimensional propagation velocity in the $\ell$-space, given by the Eqs. (4) through (7); $S$ represents the conventional source terms for the energy balance equation. For brevity of notation the dependence of spectra and source terms on x and $t$ is omitted in the following.

The first term in Eq. (9) describes the local rate of change of the variance density. The second term describes propagation in the x-space including bottom- and current-induced straining (commonly known as shoaling for bottom-induced straining). The third term describes the redistribution of energy density over the spectrum. In the directions space it corresponds to a change of direction of a spectral component (refraction). In the $\omega$-space it corresponds to a change of absolute frequency due to the unsteadiness of depth and current (e.g., Barber 1949). In the wavenumber space it corresponds to a change of wavenumber due to straining of the wave field.

A review of source terms as occur on the right hand side of Eq. (9) is given by e.g., Hasselmann (1968), Phillips (1977), LeBlond and Mysak (1978) and Sobey (1986). The source term $S(\ell)$ is generally divided in three separate terms, i.e., wind input $S_{in}(\ell)$, nonlinear wave–wave interactions $S_{nl}(\ell)$ and dissipation $S_{ds}(\ell)$:

$$S(\ell) = S_{in}(\ell) + S_{nl}(\ell) + S_{ds}(\ell). \quad (10)$$

Source terms are conventionally formulated without considering currents. If (slowly varying) currents are considered, the conventional formulations are valid in a frame of reference moving with the current. They merely need to be transformed to a fixed frame of reference with some minor adaptations to account for the wind speed being defined in the moving frame and for effects of currents on the bottom boundary layer. The formulation of all source terms used in this study (except for part of the dissipation term) are taken directly from the WAM model (WAMDI Group 1988).

In the WAM model the wind input is modeled solely with the expression for exponential growth of Snyder et al. (1981). Rescaled with the wind friction velocity $U^*$ (Charnock 1955) their expression becomes (Komen et al. 1984):

$$S_{in}(\ell) = \max\left[0, \left(0.25\rho_r \times \left(\frac{28U^*}{\sigma/k}\cos(\theta - \theta_w) - 1\right)\right)\right]\sigma F(\ell), \quad (11)$$

$$U^* = U_{10,r}\sqrt{(0.8 + 0.065U_{10,r})10^{-3}}, \quad (12)$$

where $\rho_r$ is the density of air divided by density of water, $\theta_w$ is the wind direction and $U_{10,r}$ is the wind speed in m s$^{-1}$ at ten meters above the mean sea surface, relative to the mean current. The theory of linear growth (Phillips 1957) is ignored, since exponential growth dominates rapidly.

In the process of wave generation, nonlinear resonant wave–wave interactions (Hasselmann 1960; Phillips 1960) are important since they migrate the peak of the spectrum to lower frequencies. For deep water at least four wave components (a so-called quadruplet) are needed to satisfy the resonance conditions

$$\mathbf{k}_1 + \mathbf{k}_2 - \mathbf{k}_3 = \mathbf{k}_4$$
$$\sigma_1 + \sigma_2 - \sigma_3 = \sigma_4 \quad (13)$$

where the components 1, 2 and 3 exchange energy with component 4. The expressions for the corresponding exchange of energy are rather complex and are not reproduced here (see e.g., Hasselmann 1968; Sell and Hasselmann 1972; Hasselmann and Hasselmann

1985). For shallow water, the deep water expressions are simply scaled (see below).

For waves in shelf seas away from the coast, two mechanisms of wave energy dissipation can be distinguished: i.e., whitecapping, ($S_{ds,w}$) and energy dissipation due to wave–bottom interactions ($S_{ds,b}$)

$$S_{ds} = S_{ds,w} + S_{ds,b}. \quad (14)$$

The expressions for the whitecapping source term ($S_{ds,w}$) of Komen et al. (1984), as reformulated by the WAMDI Group (1988), is used:

$$S_{ds,w}(\ell) = -2.36 \times 10^{-5} \hat{\sigma} \frac{k}{\hat{k}} \left( \frac{\alpha}{\alpha_{PM}} \right)^2 F(\ell), \quad (15)$$

with

$$\alpha = \hat{k}^2 \iint F(\ell) d\ell,$$

$$\hat{\sigma} = (\overline{1/\sigma})^{-1}, \quad \hat{k} = (\overline{1/\sqrt{k}})^{-2},$$

where $\alpha$ is an average steepness parameter, $\alpha_{PM}$ is the value of $\alpha$ for a Pierson–Moskowitz (1964) spectrum ($\alpha = 3.02 \times 10^{-3}$) and $\hat{\sigma}$ and $\hat{k}$ are an average relative frequency and wavenumber, respectively. The overbar notation denotes straightforward averaging over the spectrum, defined for an arbitrary parameter $z$ as

$$\bar{z} = \frac{\iint z(\ell) F(\ell) d\ell}{\iint F(\ell) d\ell} \quad (16)$$

where $\bar{z}$ is the average of $z$.

Dissipation of wave energy due to wave–bottom interactions can be caused by various mechanisms. A review is given by Shemdin et al. (1978), who consider percolation, bottom motion (soft mud, vegetation) and bottom friction. For relatively fine sands as found in many shelf seas, only bottom friction is important (Shemdin et al. 1978; Weber 1989). This mechanism is still poorly understood, in particular for (irregular) waves on currents. Reanalyzing available observations, Tolman (1991b) shows that effects of currents on the (near-bottom) wave boundary layer appear to be small (i.e., much smaller than the potential effects of the variable roughness of movable beds, which is discussed below). Moreover, he shows that such effects cannot be predicted by available theoretical models. Explicit effects of currents on the wave boundary layer are therefore ignored and a no-current formulation is used here. In WAM a linear expression is used, which has several disadvantages compared to available nonlinear expressions (e.g., Cavaleri et al. 1989; Weber 1989). Instead of the linear WAM expression, the relatively simple nonlinear expression of Madsen et al. (1988) is used here. It can be written as

$$S_{ds,b}(\ell) = -\frac{8}{3\pi} f_w \frac{1}{d} \left( n - \frac{1}{2} \right) u_{b,r} F(\ell), \quad (17)$$

with

$$u_{b,r} = \left( 2 \iint \frac{\sigma^2}{\sinh^2 kd} F(\ell) d\ell \right)^{1/2},$$

where $f_w$ is a nondimensional friction factor and $u_{b,r}$ is a representative near-bottom current velocity. The friction factor $f_w$ is estimated using a slightly modified formulation of Jonsson (1963, 1966, originally for monochromatic waves; cf. Madsen et al. 1988):

$$\frac{1}{4\sqrt{f_w}} + \log_{10} \frac{1}{4\sqrt{f_w}} = m_f + \log_{10} \frac{a_{b,r}}{k_N}, \quad (18)$$

with

$$a_{b,r} = \left( 2 \iint \frac{1}{\sinh^2 kd} F(\ell) d\ell \right)^{1/2},$$

where $a_{b,r}$ is a representative near-bottom excursion amplitude, $k_N$ is a bottom roughness length scale of bottom and $m_f$ is a constant ($m_f = -0.08$ as determined experimentally for monochromatic waves by Jonsson and Carlssen 1976). Equation (18) is valid for $a_b/k_N$ larger than approximately 1, for which reason $f_w$ is taken constant for small values of $a_b/k_N$ (i.e., $f_w = 0.30$ for $a_b/k_N < 1.57$, cf. Jonsson 1980).

The major problem in estimating the friction factor $f_w$ is the estimation of the bottom roughness $k_N$. When sandy bottoms are considered, ripple formation can change the bottom roughness dramatically, from sand grain roughness (with values as low as $k_N = 200$ $\mu$m) to ripple roughness (with values as large as $k_N = 0.2$ m, e.g., Weber 1989). Grant and Madsen (1982) have proposed a formulation for the calculation of ripple geometry and corresponding bottom roughness length scales $k_N$ from sand grain roughness. This formulation shows a strong discontinuity in bottom roughness when the first ripples are formed (by monochromatic waves). This is not realistic in practical conditions because (i) the grain size is nonuniform, (ii) the depth varies in the spatial mesh of a numerical model, (iii) the waves are random, (iv) the information on actual grain sizes is poor and (v) the process of ripple formation under combined wave–current conditions is still poorly understood. Therefore the ripple geometry is not calculated explicitly. Instead the roughness length $k_N$ in Eq. (18) is taken to be constant in space and time. This constant roughness length is estimated by calibration (see section 4a).

## 3. The numerical model

### a. Introduction

The choice of the spectral parameters $\ell$ in the above has been deferred to emphasize the generality of the

spectral action balance equation. The specific choice for WAVEWATCH is $\ell = (\omega, \theta)$. This implies that in the action balance equation the change of absolute frequency due to the unsteadiness of depth and current is described by a separate term. This is convenient since the study for which the model is developed aims to investigate the effects of unsteadiness of depth and current. By switching the above term on and off in repeated calculations for otherwise identical conditions, such effects are readily investigated. To use the WAM formulations of the source terms in the absolute frequency space, a Jacobian transformation $J$ is used at the right hand side of Eq. (9). The basic equation to be solved in WAVEWATCH thus becomes

$$\frac{\partial N}{\partial t} + \nabla_x \cdot [(\mathbf{c}_g + \mathbf{U})N] + \frac{\partial}{\partial \omega}[c_\omega N] + \frac{\partial}{\partial \theta}[c_\theta N] = J\frac{S}{\sigma},$$

$$N = N(\omega, \theta, \mathbf{x}, t), \quad S = S(f_r, \theta; \mathbf{x}, t), \quad (19)$$

where

$$J = \left[2\pi\left(1 + \frac{\mathbf{U}\cdot\mathbf{e}_s}{c_g}\right)\right]^{-1}, \quad (20)$$

and where $\mathbf{e}_s$ is the unit vector in the direction $\theta$ and where $c_\omega$ and $c_\theta$ are given by Eqs. (4) and (7). To integrate the five-dimensional action balance Eq. (19) economically, a fractional step method is used (e.g., Yanenko 1971), where propagation and generation are treated separately.

*b. Propagation*

In the propagation part of WAVEWATCH, the action conservation equation, i.e. the action balance Eq. (19) without source terms, is integrated. It can be written as

$$\frac{\partial N}{\partial t} = -\frac{\partial}{\partial x_1}(c_{x_1}N) - \frac{\partial}{\partial x_2}(c_{x_2}N) - \frac{\partial}{\partial \omega}(c_\omega N) - \frac{\partial}{\partial \theta}(c_\theta N), \quad (21)$$

where $(c_{x_1}, c_{x_2}) = \mathbf{c}_g + \mathbf{U}$. The basic numerical scheme used to integrate (21) in time is an explicit predictor–corrector scheme (an iterative approximation of the Crank–Nicholson scheme, e.g., Abbott 1979), denoted here as the ICN scheme. The main advantages of this scheme are the lack of numerical diffusion and the simple way in which it can be used in a multidimensional space. The main disadvantage is the unconditionally unstable behavior for linear problems, resulting in solutions with numerical oscillations. These oscillations occur mainly when the action density distribution is badly resolved in the space considered (e.g., Van Stijn et al. 1987). The oscillations are strongly related to the occurrence of negative action and can be eliminated with minor adaptations to the basic scheme (see e.g., Van Stijn et al. 1987).

The predictor for propagation in all four spaces simultaneously is written as

$$\left[\frac{N^{n'} - N^n}{\Delta t}\right]_{i_1,i_2,i_3,i_4} = L^n_{x_1} + L^n_{x_2} + L_\omega{}^n + L_\theta{}^n, \quad (22)$$

where $n$ and $n'$ are discrete time counters denoting the old time level and the predictor, respectively and $\Delta t$ is the time increment. The terms on the right-hand side represent linear operators for propagation in the $x_1$, $x_2$, $\omega$ and $\theta$-space and $i_1$ through $i_4$ are grid counters in these spaces, respectively. The corrector is identical to the predictor, replacing $n'$ with $n+1$ and $n$ with $n''$, where $n''$ indicates an average of the previously computed acting density and the predictor estimate [i.e., $N^{n''} = 0.5(N^n + N^{n'})$].

The first term at the right hand side of Eq. (22) represents the propagation in the $x_1$-space, for which the ICN scheme is

$$L^n_{x_1} = \left[\frac{[c_{x_1}N]_{i_1-1} - [c_{x_1}N]_{i_1+1}}{2\Delta x_1}\right]^n_{i_2,i_3,i_4}. \quad (23)$$

The ICN scheme is stabilized here by combining it with a first-order upstream scheme:

$$L^n_{x_1} = \frac{1}{2\Delta x_1}\{(1+\alpha_1)[c_{x_1}N]_{i_1-1} - 2\alpha_1[c_{x_1}N]_{i_1} - (1-\alpha_1)[c_{x_1}N]_{i_1+1}\}^n_{i_2,i_3,i_4}, \quad (24)$$

where $\alpha_1$ is the upstream fraction in the $x_1$-space ($0 \leq |\alpha_1| \leq 1$, the sign of $\alpha_1$ equals the sign of $c_{x_1}$). The partial upstream character of this scheme is needed to assure stable behavior of the propagation module in situations where source terms are dominant. Based on numerical experiments, the critical upstream fraction (i.e., the minimum upstream fraction needed to assure stable behavior) is estimated from the ratio of typical time scales for propagation and generation (i.e., $\Delta x_1/c_g$ and $F/S_{in}$, respectively), as

$$\alpha_{1_c} = \min\left[1, 0.10 + 3.75\,\frac{\Delta x_1 S_{in}(f_r, \theta)}{c_g F(f_r, \theta)}\right], \quad (25)$$

The upstream fraction $\alpha$ is thus dynamically adjusted to assure that it remains small in cases where propagation is dominant (the propagation module remains approximately second order accurate in propagation dominated situation) and to assure that $\alpha$ is large enough to stabilize the propagation scheme if source terms dominate (reducing the scheme to first order accuracy). Furthermore an overall minimum upstream fraction $\alpha_{\min}$ is used to assure stability when the reso-

lution is poor (see section 4). The upstream fraction is thus calculated as

$$|\alpha_1| = \max[\alpha_{1_c}, \alpha_{\min}]. \quad (26)$$

The second term at the right-hand side of Eq. (22) represents the propagation in the $x_2$-space, which is treated identically to propagation in the $x_1$-space.

At land–sea boundaries in the x-space, an angle derivative upstream scheme is used:

$$L_{x_1}^n + L_{x_2}^n = \left[\frac{[c_{xs}N]_{\text{int}} - [c_{xs}N]_{i_1,i_2}}{\Delta s}\right]_{i_3,i_4}^n \quad (27)$$

where $\Delta s$ is the distance between the spatial grid point and the interpolation point (point 5 in Fig. 1), $c_{xs}$ is the propagation velocity in the $s$ direction ($c_{xs} = (\mathbf{c}_g + \mathbf{U}) \cdot \mathbf{e}_s$) and int is a suffix denoting the interpolation point. The flux $c_{xs}N$ at point 5 is determined by linear interpolation from the fluxes at the adjacent points, which can either be sea or land points. In land points the action fluxes are assumed to be zero.

The third term of the right hand side in Eq. (22) represents the propagation in the frequency space (i.e., the change of absolute frequency due to the unsteadiness of depth and current), which is stabilized using a limited flux approach:

$$L_\omega{}^n = \left[\frac{M_{i_3-1,i_3} - M_{i_3,i_3+1}}{\Delta\omega}\right]_{i_1,i_2,i_4}^n, \quad (28)$$

where

$$M_{j_1-1,j_2} = 0.5[(c_\omega N)_{j_1} + (c_\omega N)_{j_2}].$$

The flux between grid points $|M|$ is limited by not allowing it to be larger than $(N\Delta\omega)_u/\Delta t$, the suffix $u$ indicating the "upstream" bin in the $\omega$-space. Note that substitution of the above expressions for the fluxes $M$ in (28) (ignoring the limitation) reduces this scheme to the original ICN scheme [as in Eq. (23)].

At the boundaries in the frequency space a zero flux is assumed. For low frequencies this is allowed since $c_\omega$ [Eq. (4)] approaches zero for $\omega$ approaching zero. For high frequencies the value of $c_\omega$ is proportional to $\omega^2$. Since the high frequency saturation level of the spectrum is expected to be proportional to $\omega^{-5}$ or $\omega^{-6}$ (e.g., Phillips 1977, 1985), the flux $c_\omega N$ goes to zero for increasing frequencies. Consequently a zero flux approximation is also allowed at high frequencies.

The fourth term of the right hand side in Eq. (22) represents the propagation in the directions space (refraction) and is identical to the original ICN scheme.

$$L_\theta{}^n = \left[\frac{[c_\theta N]_{i_4-1} - [c_\theta N]_{i_4+1}}{2\Delta\theta}\right]_{i_1,i_2,i_3}^n. \quad (29)$$

The propagation in the direction space is stabilized using a conservative elimination algorithm. In this algorithm all negative action for a given frequency $\omega$ (and location $\mathbf{x}$) is removed after the propagation (predictor or corrector), and the action densities for all directions at a given location and frequency are multiplied by a constant factor to conserve $N(\omega)$. Since the directions space is a closed (circular) space no boundary points exist and no special boundary treatment is needed.

The predictor and corrector steps are performed as illustrated in Fig. 2. Note that the conservative elimination algorithm (which is used to stabilize the propagation in the directions space) removes all negative action, since it is applied after the actual propagation at each time step has been performed. Note furthermore that the adaptations to the original ICN scheme reduce the accuracy of the scheme to first order. However, this reduction occurs only locally or in cases where source terms dominate. Thus, the scheme is essentially second-order accurate when propagation dominates.

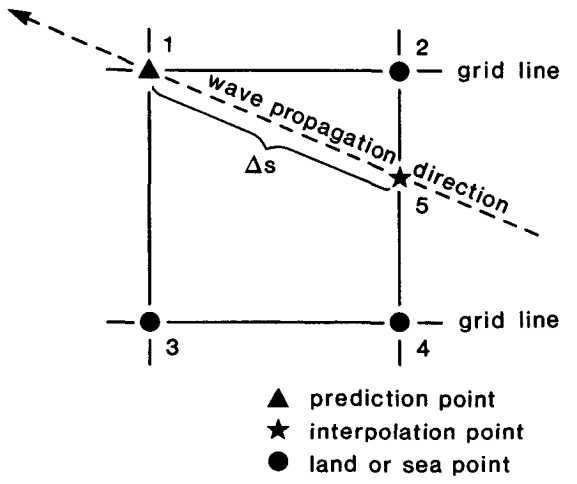


FIG. 1. Interpolation point in the angle derivative upstream scheme for boundary points in the x-space. Waves propagate from interpolation point 5 to prediction point 1.

### c. *Source terms*

In the source term part of WAVEWATCH the following reduced version of the action balance Eq. (19) is integrated:

$$\frac{\partial N}{\partial t} = \frac{S}{\sigma}. \quad (30)$$

Following WAM, source terms are calculated for the variance density spectrum $F(f_r, \theta)$. To obtain this spectrum from the (propagated) action density spectrum $N(\omega, \theta)$, a conversion is performed using the Jacobian (20).

The calculation of wind input [Eqs. (11) and (12)] and dissipation [Eqs. (14) through (18)] is straightforward algebra. The calculation of the nonlinear interactions is much more complicated and involves in-

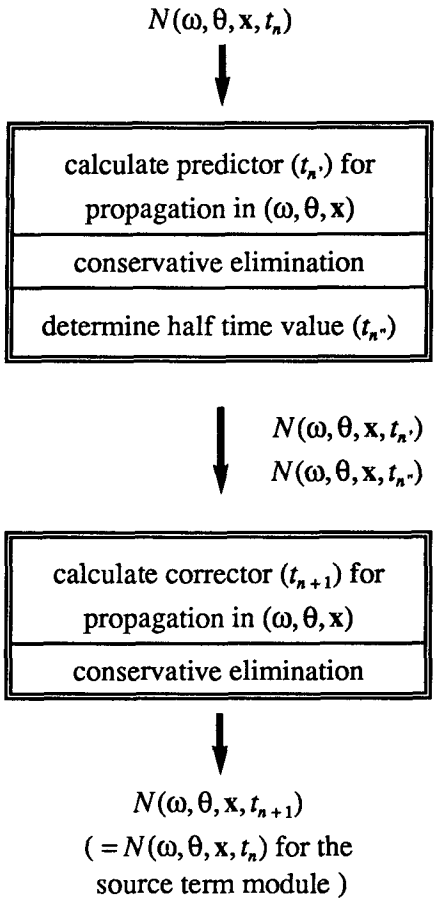


FIG. 2. Flow chart for the wave propagation scheme.

tegration over a five-dimensional continuum of resonant quadruplets. Following the WAM model, this is reduced to a two-dimensional continuum by considering a symmetrical pair of quadruplets of the following form only ($\lambda = 0.25$):

$$\sigma_2 = \sigma_1$$
$$\sigma_3 = (1+\lambda)\sigma_1$$
$$\sigma_4 = (1-\lambda)\sigma_1. \qquad (31)$$

An economic integration method for such pairs of quadruplets in deep water was developed by Hasselmann and Hasselmann (1985). For application in shallow water the expression $S_{nl}$ is scaled with a constant factor for the entire spectrum (WAMDI Group 1988). For expression for the computations of the nonlinear interactions reference is made to the above two papers.

For the integration of the source terms, a simple Euler method is used in which the change of the variance density spectrum in a single time step is calculated as

$$\Delta F(f_r, \theta) = S(f_r, \theta)\Delta t. \qquad (32)$$

This integration method is much simpler and cheaper than the semi-implicit method used in the WAM model (WAMDI Group 1988), and it appears to give similar results when combined with the stability precautions as given below (all taken directly from WAM).

Since high-frequency spectral components react rapidly to changes in wind conditions, an explicit integration method generally requires relatively small time steps to assure numerical stability (order of 1 min). Using such time steps, a third-generation model is not economically feasible. To assure numerical stability for reasonable time steps, a parametric high-frequency tail of the spectrum (i.e., $c_g^{-1}k^{-2.5}$, corresponding to $f_r^{-4}$ in deep water) is imposed for frequencies beyond the high-frequency limit $f_{r,hf}$:

$$f_{r,hf} = \max(4f_{r,\mathrm{PM}}, 2.5\bar{f}_r), \qquad (33)$$

where $f_{r,\mathrm{PM}}$ is the Pierson–Moskowitz (1964) frequency for fully developed spectra and $\bar{f}_r$ is the mean relative frequency [cf. (16)].

Furthermore, the maximum change of variance for every single spectral bin in every time step is limited to 10% of the highest spectral level that can be reached, which is estimated as the Pierson–Moskowitz equilibrium level (cf. the WAM model).

$$\max|\Delta F(f_r, \theta)| = 0.1\,\frac{\pi\epsilon_{\mathrm{PM}}}{c_g k^3}, \qquad (34)$$

where $\epsilon_{\mathrm{PM}}$ is the nondimensional energy level of the two-dimensional Pierson–Moskowitz spectrum ($\epsilon_{\mathrm{PM}} = 0.01$ as in WAM). Note that only a maximum increment is imposed, but not the shape of the spectrum itself.

The resulting change of variance density $\Delta F(f_r, \theta)$ is converted to a change of action density $\Delta N(\omega, \theta)$, again using the Jacobian (20). The change of action density is added directly to the propagated action density. Negative action that may thus arise is simply removed.

## 4. Model constants

All numerical constants in WAVEWATCH are taken from the WAM model, except for the bottom roughness length $k_N$, which is obtained by calibration. Furthermore, the effect of the minimum upstream fraction $\alpha_{\min}$ is established here.

### *a. Bottom roughness*

To calibrate the bottom roughness length scale $k_N$ in the dissipation source term for bottom friction [Eqs. (17) and (18)], a homogeneous situation without currents is considered with wind speed $U_{10} = 20$ m s$^{-1}$. For several depths $d$ (7.5 m, 15 m, 30 m, 60 m and 120 m) and roughness scales $k_N$, see Fig. 3, the equilibrium wave height $H_\infty$ and wave period $T_\infty$ have been calculated (the suffix $\infty$ indicating an "infinite" inte-

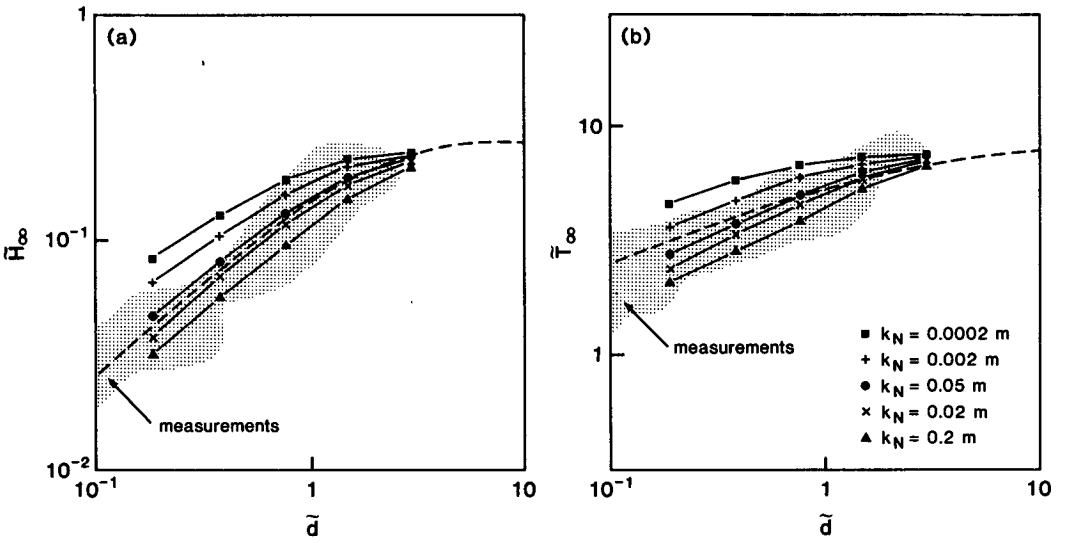


FIG. 3. Nondimensional wave height $\tilde{H}_\infty$ and wave period $\tilde{T}_\infty$ as a function of the nondimensional depth $\tilde{d}$ for several roughness scales. Full curves: WAVEWATCH; Dashed line: Krylov et al. 1976; shaded area: measurements from Holthuijsen (1980).

gration time). In these calculations spectra have been discretized using 24 directions (increments of 15°) and 26 frequencies (0.041 Hz − 0.453 Hz, $f_{i+1} = 1.1 f_i$). The time step $\Delta t$ = 15 min. for a comparison with data, the following nondimensional depth, wave height and period have been defined:

$$\tilde{d} = \frac{gd}{U_{10}^2}, \tag{35}$$

$$\tilde{H}_\infty = \frac{gH_\infty}{U_{10}^2} = \frac{4g}{U_{10}^2}\left[\int_0^{2\pi}\int_0^\infty F_\infty(\omega,\theta)d\omega d\theta\right]^{0.5}, \tag{36}$$

$$\tilde{T}_\infty = \frac{gT_\infty}{U_{10}} = \frac{g}{f_{p,\infty}U_{10}}. \tag{37}$$

For values of $k_N \approx 0.05$ m the results agree well with several recent analytical expressions for $\tilde{H}_\infty$ and $\tilde{T}_\infty$ as a function of $\tilde{d}$ (e.g., Bretschneider 1973; Krylov 1976; Groen en Dorrestein 1976). As illustration the relation of Krylov (1976) is shown in Fig. 3 (dashed line) together with the observations reviewed by Holthuijsen (1980) (shaded area).

### b. *Upstream fraction*

To establish the effects of $\alpha_{\min}$, the one-dimensional propagation along the $x$-axis of monochromatic unidirectional waves with an initial Gaussian action distribution in space is considered (deep water, no currents, no source terms, $|\alpha| = \alpha_{\min}$). Considered are the mean position ($x_m$) and spread ($\mathrm{spr}_x$) of the action distribution along the $x$-axis (i.e., the $x_1$-axis in the model):

$$x_m = \frac{m_1}{m_0}, \tag{38}$$

$$\mathrm{spr}_x = \frac{m_2}{m_0} - x_m^2, \tag{39}$$

where

$$m_n = \iiint x^n N(\omega,\theta,x)d\omega d\theta dx.$$

Both a situation with a relatively poor and a relatively good resolution are considered ($\mathrm{spr}_x = 2.0\Delta x$ and $7.5\Delta x$, respectively).

Results for various upstream fractions $\alpha$ ($=\alpha_{\min}$) are shown in Fig. 4 and Table 1 (Courant number $c_x\Delta T/\Delta x = 0.94$). The total wave action in the model (i.e., integrated over $\omega$, $\theta$ and $x$) is very nearly conserved (changes less than 0.1%), as long as no action crosses the boundaries of the numerical model. In Table 1 test results for integrated parameters other than the total action are presented. Presented are the mean position $x_m$ and the spread, $\mathrm{spr}_x$, both in terms of the mesh size $\Delta x$.

Figure 4a and the first columns of Table 1 show that only a small upstream fraction (e.g., $\alpha = 0.1$) is needed to remove the tail of the spatial action distribution, provided that the mesh size in the model is small enough to represent the spatial action distribution well. Errors in $x_m$ and $\mathrm{spr}_x$ as introduced by the upstream scheme are small. For smaller Courant numbers the ICN scheme shows similar errors in $x_m$ and $\mathrm{spr}_x$, with less tail forming (test results not presented here).

In a situation with a poor resolution (Fig. 4b, right-hand side of Table 1) the ICN scheme with $\alpha$ = 0

shows unstable behavior (not shown in the figure). A small upstream fraction ($\alpha = 0.05$–$0.10$) is sufficient to stabilize the scheme, but will not remove the tail and negative action. In the case considered here an upstream fraction $\alpha = 0.25$ is needed to remove all negative action, introducing significant diffusion (error in spread) but no significant error in the mean convection velocity (or in $x_m$).

These results indicate that the smallest value of $\alpha$ as given by Eq. (26) (i.e., $\alpha = 0.10$) suffices to stabilize the numerical scheme and to remove all negative action for resolutions where $\text{spr}_x$ is larger than approximately $5\Delta x$. For poorer resolutions, the minimum upstream fraction $\alpha_{\min}$ has to be chosen larger (e.g., $\alpha_{\min} \approx 0.25$ for $\text{spr}_x \approx 2\Delta x$). Note that negative action occurring due to a (locally) poor resolution will be removed by the conservative elimination algorithm (see Fig. 2).

## 5. Example calculations

### a. *Plane beach refraction*

In most papers considering refraction, the numerical representation of refraction is tested using a plane beach refraction test (e.g., Golding 1983; Sakai et al. 1983; Gao 1986). Results of such a test are also presented here. A one-dimensional beach with slope $10^{-3}$ is considered on a regular grid ($\Delta x_1 = 5$ km) in the depth range from 5 to 50 m. The directional resolution in the spectra $\Delta\theta = 15°$, the time step $\Delta t = 15$ min and the upstream fraction $\alpha = 0.4$. This fraction is taken relatively large to exaggerate errors. To test relatively coarse and fine directional resolutions, two monochromatic, short-crested cases have been considered (wave period of 10 s). Case I concerns a small directional spread ($\cos^{12}(\theta - \bar{\theta})$) and strongly oblique incidence at the deep water boundary ($\bar{\theta} = 45°$). In case II a situation is considered with a large directional spread ($\cos^2(\theta - \bar{\theta})$) and near-normal incidence at the deep water boundary ($\bar{\theta} = 15°$). The mean direction $\bar{\theta}$ and the directional spread, $\text{spr}_{\bar{\theta}}$, are defined as (Kuik et al. 1988):

$$\bar{\theta} = \arctan \frac{b}{a}, \tag{40}$$

$$\text{spr}_{\bar{\theta}} = [2(1 - \sqrt{a^2 + b^2})]^{1/2}, \tag{41}$$

where

$$a = E^{-1} \int \cos\theta F(\omega_0, \theta) d\theta,$$

$$b = E^{-1} \int \sin\theta F(\omega_0, \theta) d\theta, \quad E = \int F(\omega_0, \theta) d\theta$$

($a$ and $b$ are the first two Fourier components of the directional distribution, $\omega_0$ is the frequency of the monochromatic waves).

For the simple geometry of a plane beach, semi-analytical solutions for the action density distribution as a function of the local depth $d$ are available. Considering a situation with a bottom slope in $x_1$ direction only, the angle as a function of depth is calculated using Snel's[2] law:

$$\frac{\sin\theta}{c} = \text{const}, \quad c = \frac{\sigma}{k}, \tag{42}$$

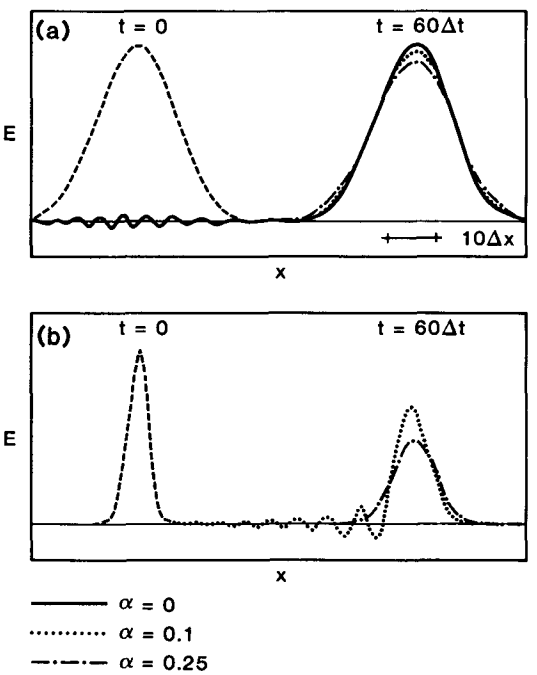


FIG. 4. One-dimensional deep-water wave propagation without currents for various upstream fractions $\alpha$ (Courant number 0.94): (a) good resolution $\text{spr}_x = 7.5\Delta x$ and (b) poor resolution $\text{spr}_x = 2.0\Delta x$.

TABLE 1. Results of one-dimensional deep-water propagation tests without currents. Courant number $c_g\Delta t/\Delta x = 0.94$, 60 time steps, $x_m/\Delta x = 21.00$ initially.

| | Good resolution | | Poor resolution | |
|---|---|---|---|---|
| $\alpha$ (−) | $x_m/\Delta x$ (−) | $\text{spr}_x/\Delta x$ (−) | $x_m/\Delta x$ (−) | $\text{spr}_x/\Delta x$ (−) |
| 0.00 | 77.24 | 7.36 | unstable | unstable |
| 0.10 | 77.22 | 7.73 | 77.21 | 3.12 |
| 0.25 | 77.20 | 8.31 | 77.22 | 4.25 |
| 0.50 | 77.12 | 8.92 | 77.22 | 5.67 |
| 1.00 | 76.90 | 10.09 | 77.18 | 7.71 |
| Exact | 77.21 | 7.50 | 77.21 | 2.00 |

[2] Willebrordus Snel van Royen lived and worked in the low countries (1580–1626). In his scientific publications, he used the Latinized name Snellius. In English literature his name is generally used in the incorrectly de-latinized form of Snell.

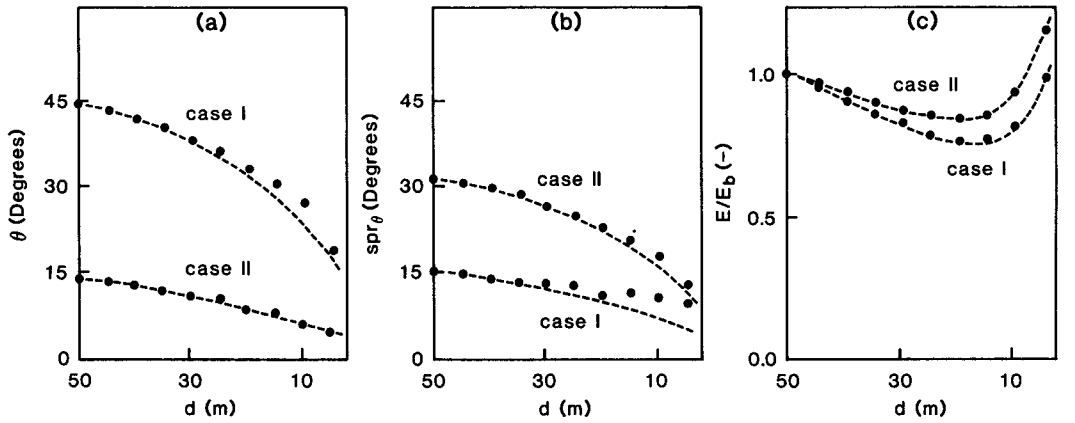


FIG. 5. Depth refraction on a plane beach, mean wave parameters as a function of the depth. (a) Mean direction $\bar{\theta}$. (b) Directional spread $\text{spr}_\theta$. (c) Total variance $E$ normalized with variance at deep water boundary $E_b$. Dashed lines: analytical solution; symbols: numerical results.

where the constant is determined from the (deep water) boundary conditions. When the directional distribution at the deep-water boundary is known at intervals $\Delta\theta'$ ($\Delta\theta' \ll \Delta\theta$, grid counter $j$), the exact solution for the directional distribution at arbitrary depths is estimated as:

$$F(\theta_j) = F(\theta_{0,j}) \frac{2\Delta\theta'}{\theta_{j+1} - \theta_{j-1}} \left[ \frac{c_{g,o}}{c_g} \frac{\cos\theta_{0,j}}{\cos\theta_j} \right], \quad (43)$$

where the suffix 0 indicates known parameter values at the deep-water boundary.

Results for both cases are shown in Figs. 5 and 6. In case I (poor directional resolution) the mean direction $\bar{\theta}$ and total energy $E$ ($= \int\int F(\omega, \theta) d\omega d\theta$) as obtained from the numerical model show good agreement with the semi-analytical solutions ($\Delta\theta' = 1°$). The directional spread $\text{spr}_\theta$, however, is represented poorly. This can be explained by the extremely small directional spread compared to the directional increment $\text{spr}_\theta$ (the spread is even smaller than the directional increment $\Delta\theta$). Case II, with a much better resolution, shows good agreement between numerical and analytical results.

It should be noted that in published models the propagation in the directional space is usually modeled with a first-order upstream scheme (e.g., Golding 1983; Sakai et al. 1983; Gao 1986; WAMDI Group 1988). Test results presented in several of these papers show acceptable results for the mean wave direction. However, these results do not show the weak point of first-order upstream schemes, being the introduction of numerical diffusion and the corresponding smoothing and broadening of the directional distribution. Since directional distributions and/or directional spreads are not presented in the above papers, effects of numerical diffusion cannot be estimated from the data presented in the above papers.

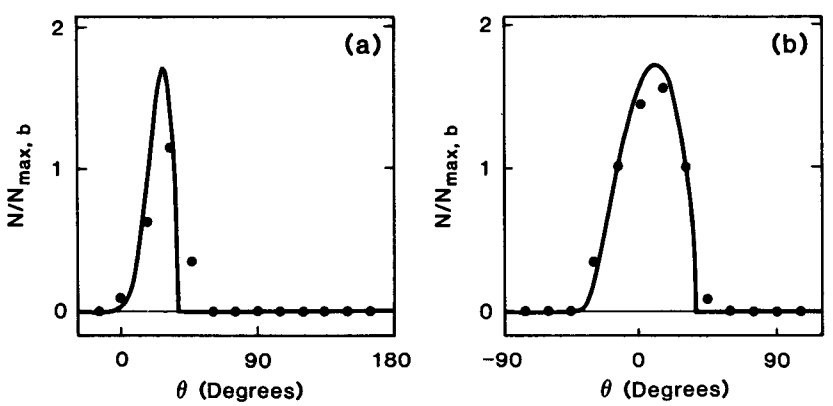


FIG. 6. Depth refraction on a plane beach, directional distribution for $d = 10$ m. Solid lines: analytical solution; symbols: numerical results. (a) Case I: poor resolution. (b) Case II: good resolution.

*b. Waves in a Gulf Stream ring*

In this section wind wave propagation over the Gulf Stream ring of Fig. 7a is considered (deep water), to illustrate advantages of the present grid model over ray models and to illustrate the effects of the random character of waves and of source terms. This case is discussed in detail by Holthuijsen and Tolman (1991). To illustrate the effects of short-crestedness and of wind, three cases have been considered. In the first case monochromatic, long-crested swell with a period of 14 s is propagated over the ring using a conventional ray technique (Fig. 7b). In the second case swell with a narrow banded spectrum is propagated over the ring with the present model neglecting source terms (Fig. 7c). The mean period at the upwave boundary is 14 s and the significant wave height $H_s = 1.99$ m.

$$H_s = 4\left(\int\int F(\omega, \theta)d\omega d\theta\right)^{1/2} \qquad (44)$$

The spectrum has a Gaussian distribution in the frequency space ($\mathrm{spr}_f = 0.1\bar{f}$) and a $\cos^{20}(\theta - \bar{\theta})$ directional distribution. In the third case wind waves are considered with a wind speed of 20 m s$^{-1}$. At the upwind boundary a JONSWAP spectrum (Hasselmann et al. 1973) was applied with a significant wave height $H_s = 8.1$ m and a spectral peak frequency corresponding to a period of 14 s.

In Fig. 7b wave rays for the monochromatic swell case are presented. Similar figures have been presented by several authors (e.g., Dobson and Irvine 1983; Mapp et al. 1985; Mathiesen 1987). Of these authors, only Mathiesen presents spatial distributions of the wave height.

In Fig. 7c wave heights and mean wave directions are presented for the more realistic narrow banded swell of the second case (obtained from spectra calculated by the present model). This figure shows significant current-induced variations of the wave height in locations where the rays of Fig. 7b cross (increase up to

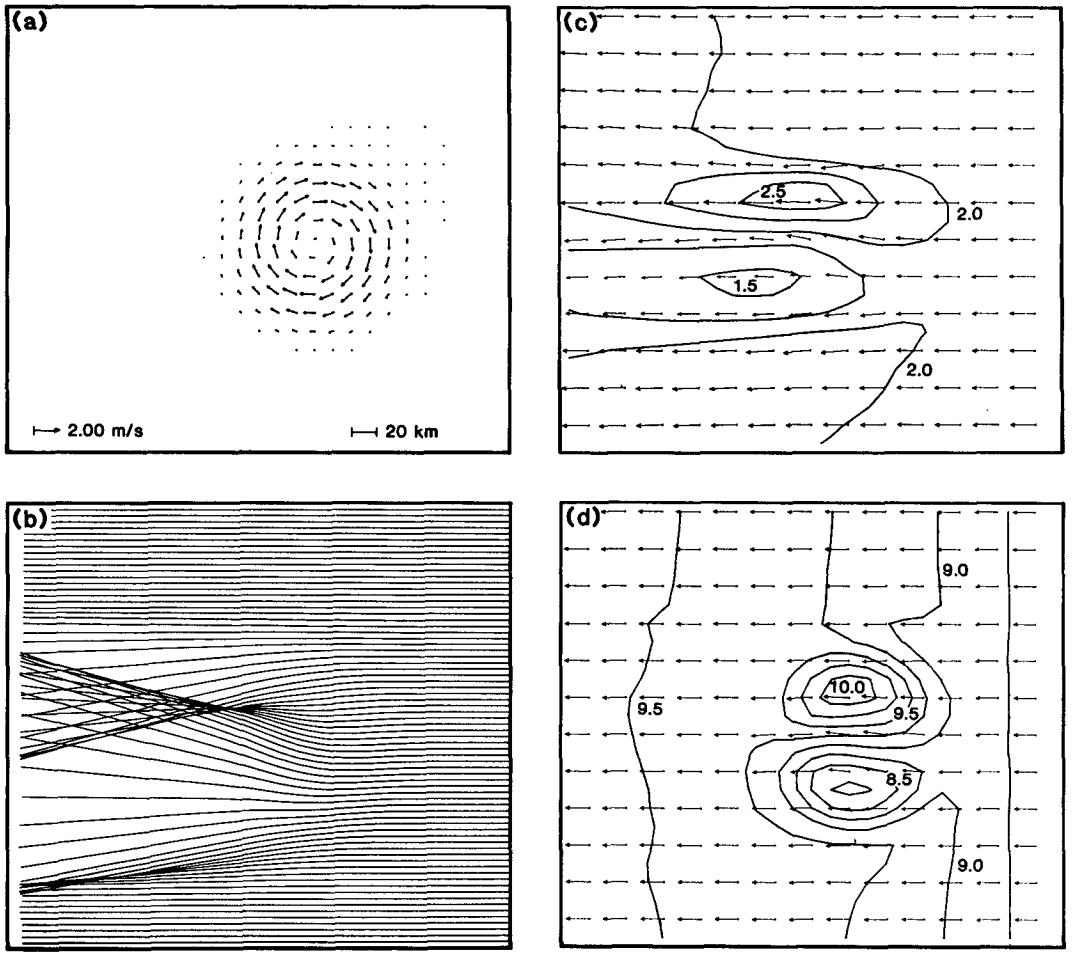


FIG. 7. Waves propagating over a Gulf Stream ring. (a) Current vectors. (b) Rays for monochromatic, long-crested swell with $T = 14$ s. (c) Mean wave directions and isolines of significant wave heights for irregular, short-crested swell with $\bar{T}_\alpha \approx 14$ s. (d) Like (c), wind sea with $U_{10} = 20$ m s$^{-1}$, near full development. Vector points in current/mean wave propagation direction.

2.7 m) or diverge (decrease down to 1.4 m). Furthermore bimodal spectra are found in several locations where the rays of Fig. 7b suggest that cross-seas occur (for figures see Holthuijsen and Tolman 1991). Whereas Fig. 7b suggests that the effects of the ring spread over a large area "downwave" of the ring, Fig. 7c indicates that effects of the ring are limited to a more confined area, and lessen with increasing distance to the ring. This is probably caused by (a) the short-crested and random character of the waves and (b) the divergence of the (refracted) rays behind the ring.

In Fig. 7d wave heights and directions for the wind sea case are presented. Whereas wave height modulations still are significant, the effects of the ring are limited to the area of the ring, and there are no lasting effects downwave of the ring. An intercomparison of Figs. 7c and 7d clearly shows that the ring has a different influence on wind seas in active generation conditions than on swell without wind.

### c. *North Sea wind waves*

In this section some hindcast results for a series of moderate southwesterly storms on the southern North Sea of 1–4 January 1988 are presented. These storms are caused by a series of depressions traveling in a NE direction over Scotland, with wind speeds up to Beaufort 7. Since this case is merely meant to illustrate features of WAVEWATCH, in particular, effects of depth and current unsteadiness, the presentation and discussion of results will be limited to a single location (i.e., Euro-0, see Fig. 8). A more extensive presentation of this case is given by Tolman (1991a).

Depth, current and wind data for Euro-0 are gathered in Fig. 9. The wind fields consist of forecast UK6 wind fields of the British Meteorological Office. The currents and water levels have been calculated using a depth-integrated tide and surge model (DUCHESS, e.g., Wang 1989), using both wind forcing and tidal constituents at the open ocean boundaries (typically 6 constituents, taken from Voogt 1985). Water levels and currents as presented in Fig. 9 are clearly tide dominated with a negligible effect of storm surges. Wind wave spectra have been hindcasted using the spectral discretization as in the calibration of the bottom roughness length scale, spatial resolution $\Delta x_1 = \Delta x_2 = 24$ km and a time step $\Delta t = 15$ min.

In Fig. 10 the significant wave height $H_s$ [Eq. (44)], the mean absolute and relative period $T_a$ and $T_r$ and the mean wave length $L$ are presented.

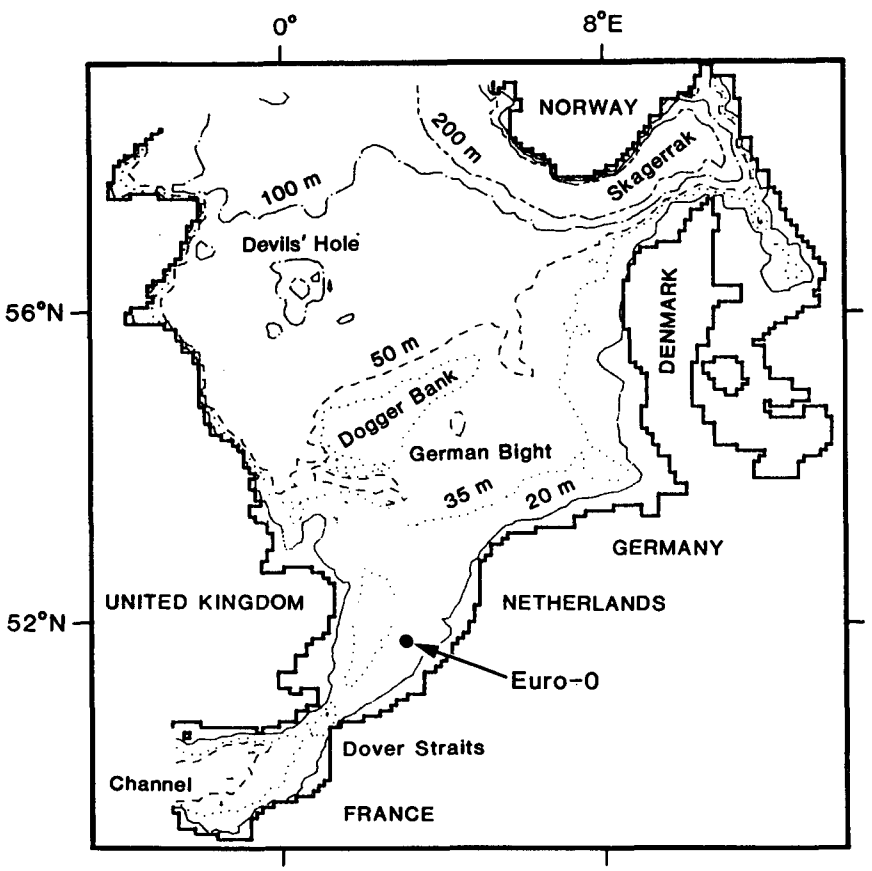


FIG. 8. The North Sea, bottom levels and location Euro-0.

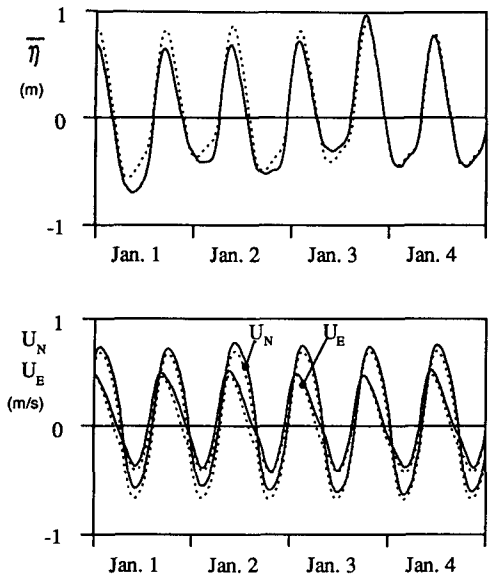


FIG. 9. Water levels $\eta$ and current velocity components in northern and eastern directions ($U_N$ and $U_E$, respectively) for location Euro-0 on 1–4 Jan 1988. Solid lines with wind forcing, dotted lines without wind forcing.

$$T_a = \frac{\overline{2\pi}}{\omega}, \tag{45}$$

$$T_r = \frac{\overline{2\pi}}{\sigma}, \tag{46}$$

$$L = \frac{\overline{2\pi}}{k}. \tag{47}$$

The overbar notation denotes an average over $F(\omega, \theta)$ as in (16). Results are presented as obtained with and without tides (solid lines and dotted lines, respectively). Effects of the tides (i.e., the difference between the solid and dotted lines), are small but distinct in all parameters of Fig. 10. The mean wave direction (not presented here), showed negligible tidal effects (tide-induced modulations of less than 1°). Also presented in Fig. 10 are numerical results as obtained with tides, but neglecting the specific effects of its unsteadiness (i.e., with $c_\omega \equiv 0$, dashed lines). The differences between the dashed and solid lines indicate that the effects of unsteadiness are important within the wave–current interactions, in particular for predicted relative periods and wave lengths.

For the case and location considered here observed wave data (WAVEC buoy, e.g., Van der Vlugt, 1984) were available. To compare the relatively small effects of tides on waves with data, such effects have been isolated. In the hindcast the effects are isolated by considering the differences between the calculations with and without tides (i.e., dotted and solid lines of Fig. 10). In the observations, tidal influences are restricted to certain frequency bands. Modulations within this frequency band can be isolated from the observations using filtering techniques, which, however, do not identify the origin of the modulations. Apart from the tides, the wind is obviously a potentially important source of such modulations, in particular since calculated tide-induced modulations are relatively small. Since sufficiently accurate (high resolution) wind fields are not available to calculate wind-induced modulations, they can only be estimated as the difference between the calculated (tide-induced) modulations and the observed (tide- and wind-induced) modulations. The apparently wind-induced modulations can in turn be compared to observed (filtered) wind speed variations to assess their correlation.

Observed and calculated modulations of the significant wave height and the absolute period ($\Delta H_s$ and $\Delta T_a$, respectively) are presented in Fig. 11. Modula-

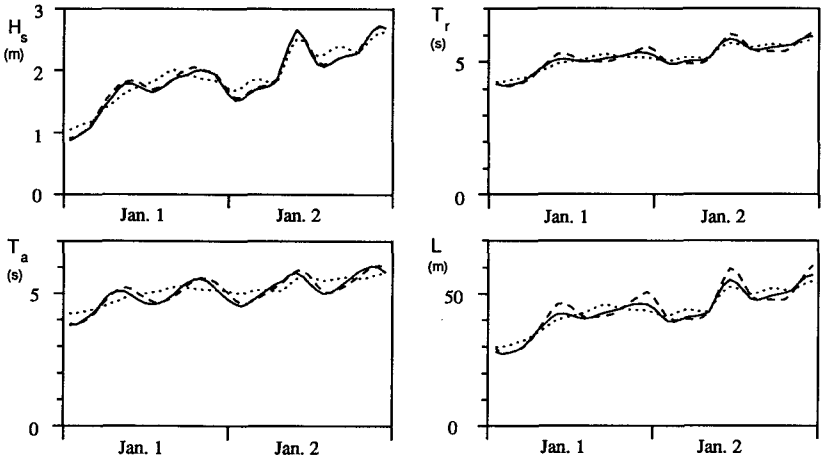


FIG. 10. Mean wave parameters for Euro-0 on 1 and 2 Jan 1988. Solid lines with tides; dotted lines without tides; dashed lines with tides, neglecting effects of unsteadiness.

tions with periods between approximately 9 and 15 h have been isolated from the observations using running averages. Figure 11 shows large differences between observed and calculated wave modulations, in particular for the modulation of the wave height. Such differences may well be caused by the wind (as discussed above). To investigate whether this is true, the above differences between observed and calculated modulations of mean wave parameters are compared with filtered wind speeds (same frequency band) in Fig. 12. To allow for a direct comparison, wind and wave data in this figure have been normalized with their rms value for the period considered. The high correlation between filtered wind speeds and possibly wind-induced modulations of wave parameters of Fig. 12 indicates that the differences between observed and calculated modulations of wave parameters of Fig. 11 are indeed probably wind-induced, and not caused by model errors.

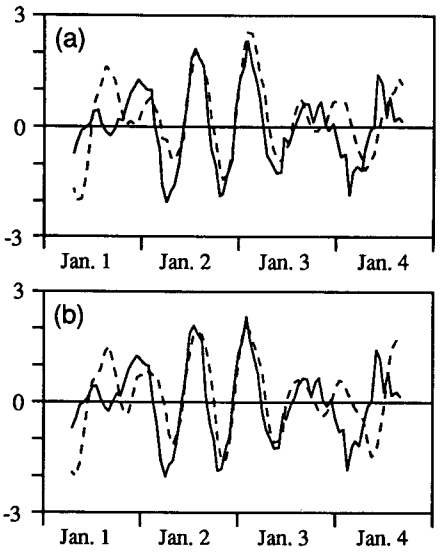


FIG. 12. Normalized wind speed variations (solid lines) and apparently wind induced modulations of mean wave parameters (dashed lines, difference between observed and calculated modulations) for Euro-0 on 1–4 Jan 1988. (a) The significant wave height. (b) The mean absolute wave period.

## 6. Discussion

The model presented here incorporates all relevant effects of wave–current interactions for slowly varying current fields as well as explicit formulations for wave growth, dissipation and nonlinear wave–wave interactions. The results for the Gulf Stream ring indicate that it is difficult to assess the effects of a current on short-crested swell or wind seas from conventional ray computations. Furthermore, effects of wave generation and of wave–current interactions might be important for wind seas propagating over large-scale deep-ocean current systems such as the Gulf Stream, the Agulhas Current or the Kuroshio (this will be discussed in detail by Holthuijsen and Tolman 1991). Up to now, however, wave–current interactions for large-scale current fields have been studied by considering conservative propagation without source terms only (e.g., Mathiesen 1987; Irvine and Tilley 1988; Liu et al. 1989; Yamaguchi and Hatada 1990).

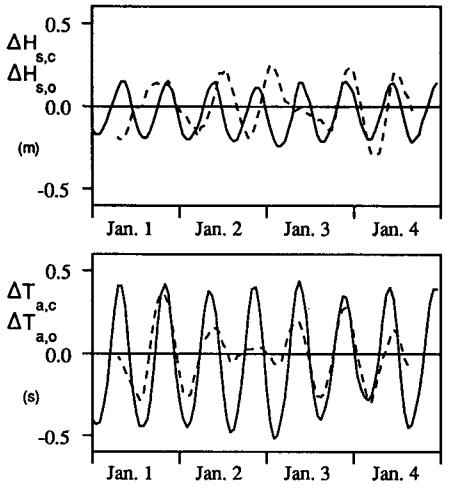


FIG. 11. Calculated and observed modulations (solid and dashed lines, respectively) of the significant wave height ($\Delta H_s$) and the mean absolute period ($\Delta T_a$) for Euro-0 on 1–4 Jan 1988.

The results for the North Sea hindcast presented here indicate that the unsteadiness has a significant influence on calculated modulations of mean wave parameters (in particular the mean wave length). This is in qualitative agreement with previous analytical results for conservative propagation in highly idealized cases (Tolman 1990b). The comparison of model results with data in the North Sea case shows promising results; the model seems to describe current-induced modulations correctly. However, the occurrence of wind-induced modulations with similar magnitude as calculated current-induced modulations hampers the objective analysis of the quality of the model results.

With respect to the present model formulation two remarks have to be made. First, the model presented here is defined on a plane grid, introducing projection errors when propagation over a sphere is considered. This limits the applicability of the model to areas of 1000 to 2000 km in diameter. Such a model size is sufficient to describe most shelf seas. For application on the scale of oceans spherical propagation has to be considered, slightly modifying the rectilinear propagation terms and introducing an additional refraction term (e.g., WAMDI Group 1988). Since refraction is already implemented in the model, this represents a minor adaptation to the model. Second, a model formulated in terms of the spectrum $N(k, \theta)$ might be preferred to a model formulated in terms of $N(\omega, \theta)$ (as presented here). The former spectrum has better invariance properties, requires no interpolations be-

tween the propagation and source terms part of the model, and results in easier solutions of the dispersion relation.

*Acknowledgments.* The author acknowledges with pleasure that S. Glenn of Harvard University supplied the Gulf Stream current field and that J. Dekker of Delft Hydraulics performed the ray calculations (Fig. 7b). The Dutch Ministry of Public Works and Transportation (Rijkswaterstaat) supplied the bottom grid for the North Sea and the boundary conditions for the depth and current model used for the North Sea hindcast and that the Royal Netherlands Meteorological Institute (KNMI) made the UK6 wind fields available. In particular the help of J. de Ronde, R. van Dijk (Rijkswaterstaat), H. W. Riepma and E. Bouws (KNMI) was greatly appreciated. Furthermore the author thanks L. H. Holthuijsen and J. A. Battjes (Delft University of Technology) for reading early drafts of this paper and L. Rumburg (NASA/GSFC) for her help in preparing the figures. Part of this manuscript has been written while the author held a National Research Council–NASA Research Associateship.

## REFERENCES

Abbott, M. B., 1979: *Computational Hydraulics.* Pitman, 324 pp.

Barber, N. F., 1949: Behaviour of waves on tidal streams. *Proc. Roy. Soc. London,* **A198,** 81–93.

Bretherthon, F. P., and C. J. R. Garrett, 1968: Wave trains in inhomogeneous moving media. *Proc. Roy. Soc. London,* **A302,** 529–554.

Bretschneider, C. L., 1973: Shore Protection Manual, U.S. Army CERC, Corps of Engineers, Tech. Rep. No. 4.

Cavaleri, L., L. Bertotti and P. Lionello, 1989: Shallow water application of the third-generation WAM wave model. *J. Geophys. Res.,* **94**(C6), 8111–8124.

Charnock, H., 1955: Wind stress on a water surface. *Quart. J. Roy. Meteor. Soc.,* **81,** 639–640.

Chen, Y. H., and H. Wang, 1983: Numerical model for nonstationary shallow water wave spectral transformations. *J. Geophys. Res.,* **88**(C14), 9851–9863.

Christoffersen, J. B., 1982: Current depth refraction of dissipative water waves. Institute of Hydrodynamics and Hydraulic Engineering, Technical University of Denmark, Series Paper No. 30.

Dingemans, M. W., M. J. F. Stive, J. Bosma, H. J. de Vriend and J. A. Vogel, 1986: Directional near-shore wave propagation and induced currents. *Proc. 20th Int. Conf. Coastal Engineering,* Taipei, ASCE, 1092–1106.

Dobson, E. B., and D. E. Irvine, 1983: Investigation of Gulf Stream ring detection with spaceborne altimeter using mean sea height, wave height, and radar cross section. The Johns Hopkins University, Applied Physics Laboratory, Space Department, Rep. JHU/APL S1R3U-005, 51 pp.

Gao, Q. D., 1986: Extension of the third generation ocean wave model with refraction. Scientific Report WR 86-5, Royal Netherlands Meteorological Institute.

Gelci, R., H. Cazalé and J. Vassal, 1956: Utilization des diagrammes de propagation à la prévision énergétique de la houle. *Bulletin d' Information du Commité Central d' Océanographie et d' Études des Côtes,* **8,** 169–197.

——, —— and ——, 1957: Prévision de la haule. La méthode des densités spectroangulaires. *Bulletin d' Information du Commité Central d' Océanographie et d' Études des Côtes,* **9,** 416–435.

Golding, B., 1983: A wave prediction system for real time sea state forecasting. *Quart. J. Roy. Meteor. Soc.,* **109,** 393–416.

Grant, W. D., and O. S. Madsen, 1982: Movable bed roughness in unsteady oscillatory flow. *J. Geophys. Res.,* **87**(C1), 469–481.

Groen, P., and R. Dorrestein, 1976: *Zeegolven.* 3rd ed. Staatsuitgeverij, 124 pp. (in Dutch).

Hasselmann, K., 1960: Grundgleichungen der Seegangsvoraussage. *Schiffstechnik,* **7,** heft 39, 191–195.

——, 1968: Weak-interaction theory of ocean waves. *Basic Developments in Fluid Mechanics,* **2,** M. Holt, Ed., Academic Press, 117–182.

——, and S. Hasselmann, 1985: Computations and parameterizations of the nonlinear energy transfer in a gravity-wave spectrum. Part I: A new method for efficient computations of the exact nonlinear transfer integral. *J. Phys. Oceanogr.,* **15,** 1369–1377.

——, T. P. Barnett, E. Bouws, H. Carlson, D. E. Cartwright K. Enke, J. A. Ewing, H. Gienapp, D. E. Hasselmann, P. Kruseman, A. Meerburg, P. Müller, D. J. Olbers, K. Richter, W. Sell and H. Walden, 1973: Measurements of wind-wave growth and swell decay during the Joint North Sea Wave Project (JONSWAP). *Ergänzungsheft zur Deutschen Hydrographischen Zeitschrift,* Reihe A (8°) Nr. **12,** 95 pp.

Holthuijsen, L. H., 1980: *Methoden voor Golfvoorspelling.* Part I and II. Technische Adviescommissie voor de Waterkeringen, 141 pp. (in Dutch).

——, N. Booij and T. H. C. Herbers, 1989: A prediction model for stationary, short crested waves in shallow water with ambient currents. *Coastal Eng.,* **13,** 23–54.

——, and H. L. Tolman, 1991: Effects of the Gulf Stream on ocean waves. *J. Geophys. Res.,* in press.

Irvine, D. E., and D. G. Tilley, 1988: Ocean wave directional spectra and wave-current interaction in the Agulhas from the Shuttle imaging radar-B synthetic aperture radar. *J. Geophys. Res.,* **93**(C12), 15 389–15 401.

Jonsson, I. G., 1963: Wave boundary layers. *Proc. 10th Congr. IAHR,* London, 85–92.

——, 1966: Wave boundary layers and friction factors. *Proc. 10th International Conf. on Coastal Engineering,* Tokyo, ASCE, 127–148.

——, 1980: A new approach to oscillatory rough turbulent boundary layers. *Ocean Eng.,* **7,** 109–152.

——, 1990: Wave-current interactions. *The Sea, Vol. 9: Ocean Engineering Science,* B. Le Mehaute and D. M. Hanes, Eds., Wiley.

——, and N. A. Carlsen, 1976: Experimental and theoretical investigations in an oscillatory turbulent boundary layer. *J. Hydraul. Res.* **14,** 45–60.

Komen, G. J., S. Hasselmann and K. Hasselmann, 1984: On the existence of a fully developed wind-sea spectrum. *J. Phys. Oceanogr.,* **14,** 1271–1285.

Krylov, Yu. M., S. S. Strekalov and V. F. Tsyplukhin, 1976: Wind waves and their influence on structures (in Russian). *Hydrometoizdat.*

Kuik, A. J., G. Ph. van Vledder and L. H. Holthuijsen, 1988: A method for the routine analysis of pitch-and-roll buoy wave data. *J. Phys. Oceanogr.,* **18,** 1020–1034.

LeBlond, P. H., and L. A. Mysak, 1978: *Waves in the Ocean.* Elsevier, 602 pp.

Longuet-Higgins, M. S., and R. W. Stewart, 1960: Changes in the form of short gravity waves on long waves and tidal currents. *J. Fluid Mech.,* **8,** 565–583.

——, and ——, 1961: The changes in amplitude of short gravity waves on steady nonuniform currents. *J. Fluid Mech.,* **13,** 481–504.

——, and ——, 1962: Radiation stress and mass transport in gravity waves, with application to 'surf-beats.' *J. Fluid Mech.,* **10,** 529–549.

Liu, A. K., F. C. Jackson, E. J. Walsh and C. Y. Peng, 1989: A case study of wave-current interaction near an oceanic front. *J. Geophys. Res.,* **94**(C11), 16 189–16 200.

Madsen, O. S., Y.-K. Poon and H. C. Graber, 1988b: Spectral wave attenuation by bottom friction: theory. *Proc. 21st Int. Conf. on Coastal Engineering,* Malaga, ASCE, 492–504.

Mathiesen, M., 1987: Wave refraction by a current whirl. *J. Geophys. Res.,* **92**(C4), 3905–3912.

Mapp, G. R., C. S. Welch and J. C. Munday, 1985: Wave refraction by warm core rings. *J. Geophys. Res.*, **90**(C4), 7153–7162.

Mei, C. C., 1983: *The Applied Dynamics of Ocean Surface Waves.* Wiley, 740 pp.

Peregrine, D. H., 1976: Interaction of water and waves and currents. *Adv. Appl. Mech.*, **16**, 9–117.

——, and I. G. Jonsson, 1983: Interaction of waves and currents. Misc. Rep. No. 83-6, CERC, U.S. Army Corps of Engineering,

Phillips, O. M., 1957: On the generation of waves by turbulent wind. *J. Fluid Mech.*, **2**, 417–445.

——, 1960: On the dynamics of unsteady gravity waves of finite amplitude. Part I. *J. Fluid Mech.*, **9**, 193–217.

——, 1977: *The Dynamics of the Upper Ocean.* 2nd ed. Cambridge University Press, 336 pp.

——, 1985: Spectral and statistical properties of the equilibrium range in wind-generated gravity waves. *J. Fluid Mech.*, **156**, 505–531.

Pierson, W. J., and L. Moskowitz, 1964: A proposed spectral form for fully developed wind seas based on the similarity theory of S. A. Kitaigorodskii. *J. Geophys. Res.*, **69**, 5181–5190.

Radder, A. C., 1979: On the parabolic equation method for water-wave propagation. *J. Fluid Mech.*, **95**, 159–176.

Sakai, T., M. Koseki and Y. Iwagaki, 1983: Irregular wave refraction due to current. *J. Hydraul. Eng.*, **109**, 1203–1215.

Sell, W., and K. Hasselmann, 1974: Computation of nonlinear energy transfer for JONSWAP and empirical wind wave spectra. Rep. Inst. Geophys., University of Hamburg,

Shemdin, O., K. Hasselmann, S. V. Hsiao and K. Heterich, 1978: Nonlinear and linear bottom interaction effects in shallow water. *Turbulent fluxes through the sea surface, wave dynamics, and prediction.* NATO Conf. Ser. V, Vol. 1, 347–365.

Skovgaard, O., and I. G. Jonsson, 1976: Current depth refraction using finite elements. *Proc. 15th Int. Conf. on Coastal Engineering,* ASCE, 721–737.

Snyder, R. L., F. W. Dobson, J. A. Elliott and R. B. Long, 1981: Array measurements of atmospheric pressure fluctuations above surface gravity waves. *J. Fluid Mech.*, **102**, 1–59.

Sobey, R. J., 1986: Wind–wave prediction. *Annual Review Fluid Mech.*, Vol. 18, Annual Reviews 149–172.

Stijn, Th. L. van, J. C. H. van Eijkeren and N. Praagman, 1987: A comparison of numerical methods for air quality models. KNMI Sci. Rep. WR-87-6,

SWAMP Group, 1985: *Ocean Wave Modelling.* Plenum Press,

SWIM Group, 1985: A shallow water intercomparison of three numerical wave prediction models (SWIM). *Quart. J. Roy. Meteor. Soc.*, **111**, 1087–1112.

Tayfun, M. A., R. A. Dalrymple and C. Y. Yang, 1976: Random wave–current interaction in water of varying depth. *Ocean Eng.*, **3**, 403–420.

Tolman, H. L., 1989: The numerical model WAVEWATCH: a third generation model for the hindcasting of wind waves on tides in shelf seas. *Communications on Hydraulic and Geotechnical Engineering,* Delft University of Technology, Rep. no. 89-2, 72 pp. [ISSN 0169-6548.]

——, 1990a: Wind wave propagation in tidal seas. *Communications on Hydraulic and Geotechnical Engineering,* Delft University of Technology, Rep. no. 90-1, 135 pp. [ISSN 0169-6548].

——, 1990b: The influence of unsteady depths and currents of tides on wind wave propagation in shelf seas. *J. Phys. Oceanogr.*, **20**, 1166–1174.

——, 1991a: Effects of tides and storm surges on North Sea wind waves. *J. Phys. Oceanogr.*, **21**, 766–781.

——, 1991b: An evaluation of expressions for wave energy dissipation due to bottom friction in the presence of currents. *Coastal Eng.*, in press.

Unna, P. J., 1941: White horses. *Nature,* **148**, 226–227.

——, 1942: Waves on tidal streams. *Nature,* **149**, 219–220.

——, 1947: Sea waves. *Nature,* **159**, 239–242.

Vlugt, A. J. M. van der, 1984: Experiences with the WAVEC-buoy. *Proc. Symp. Description and Modelling of Directional Seas,* Denmark, Danish Hydraulic Institute and Danish Maritime Institute,

Voogt, L., 1985: Een getijmodel van de Noordzee gebaseerd op de JONSDAP-1976 meting. Rijkswaterstaat note WWKZ-84G.006, (in Dutch).

WAMDI Group, 1988: The WAM model—a third generation ocean wave prediction model. *J. Phys. Oceanogr.*, **18**, 1775–1810.

Wang, Z. B., 1989: Mathematical modelling of morphological processes in estuaries. *Communications on Hydraulic and Geotechnical Engineering,* Delft University of Technology, Rep. no. 89-1, 204 pp. [ISSN 0169-6548].

Weber, S. L. 1989: Surface gravity waves and turbulent bottom friction. Ph.D. thesis, University of Utrecht, the Netherlands, 128 pp.

Whitham, G. B., 1965: A general approach to linear and nonlinear dispersive waves using a Lagrangian. *J. Fluid Mech.*, **22**, 273–283.

——, 1974: *Linear and Nonlinear Waves,* Wiley, 636 pp.

Willebrand, J., 1975: Energy transport in a nonlinear and inhomogeneous random gravity wave field. *J. Fluid Mech.*, **70**, 113–126.

Yamaguchi, M., Y. Hatada and J. Hayakawa, 1989: A numerical model for refraction computation of irregular waves due to time varying currents and water depth. *Proc. of JSCE,* Vol. 405/II-11, 225–234. (in Japanese).

——, and Y. Hatada, 1990: A numerical model for refraction computation of irregular waves due to time varying currents and water depth. *Proc. 22nd Int. Conf. on Coastal Engineering,* Delft, in press.

Yanenko, N. N., 1971: *The Method of Fractional Steps.* Springer, 160 pp.